Multiparametric Quantitative MRI for the Detection of IgA Nephropathy Using Tomoelastography, DWI, and BOLD Imaging

Sophia Theresa Lang, Jing Guo, PhD,* Anne Bruns, MD,† Michael Dürr, MD,‡ Jürgen Braun, PhD,§ Bernd Hamm, MD,* Ingolf Sack, PhD,* and Stephan Rodrigo Marticorena Garcia, MD**

Objectives: The aim of this study was to noninvasively evaluate changes in renal stiffness, diffusion, and oxygenation in patients with chronic, advanced stage immunoglobulin A nephropathy (IgAN) by multiparametric magnetic resonance imaging using tomoelastography, diffusion-weighted imaging (DWI), and blood oxygen level–dependent (BOLD) imaging.

Materials and Methods: In this prospective study, 32 subjects (16 patients with biopsy-proven IgAN and 16 age- and sex-matched healthy controls) underwent multifrequency magnetic resonance elastography with tomoelastography postprocessing at 4 frequencies from 40 to 70 Hz to generate shear wave speed (meter per second) maps reflecting tissue stiffness. In addition, DWI and BOLD imaging were performed to determine the apparent diffusion coefficient in square millimeter per second and T2* relaxation time in milliseconds, respectively. Regions including the entire renal parenchyma of both kidneys were analyzed. Areas under the receiver operating characteristic (AUCs) curve were calculated to test diagnostic performance. Clinical parameters such as estimated glomerular filtration rate and protein-to-creatinine ratio were determined and correlated with imaging findings.

Results: Success rates of tomoelastography, DWI, and BOLD imaging regarding both kidneys were 100%, 91%, and 87%, respectively. Shear wave speed was decreased in IgAN (−21%, $P < 0.0001$), accompanied by lower apparent diffusion coefficient values (−12%, $P = 0.004$). BOLD imaging was not sensitive to IgAN ($P = 0.12$). Tomoelastography detected IgAN with higher diagnostic accuracy than DWI (area under the curve = 0.9 vs 0.8) and positively correlated with estimated glomerular filtration rate ($r = 0.66$, $P = 0.006$).

Conclusions: Chronic, advanced stage IgAN is associated with renal softening and restricted water diffusion. Tomoelastography is superior to DWI and BOLD imaging in detecting IgAN.

Key Words: magnetic resonance imaging, magnetic resonance elastography, tomoelastography, elastography, diffusion magnetic resonance imaging, blood oxygen level–dependent, glomerulonephritis, immunoglobulin A nephropathy, kidney, renal

(*Invest Radiol* 2019;00: 00–00)

Immunoglobulin A nephropathy (IgAN) is an autoimmune disorder with a worldwide prevalence of 2.5/100,000/year.[1,2] Aberrant synthesis of IgA1 molecules with less galactosylated *O*-glycans in the hinge region and secondary synthesis of immunoglobulin G and A autoantibodies against those with formation of immune complexes was identified as the underlying pathomechanism. It is already known that these complexes accumulate in the renal glomeruli of affected patients, initiating chronic inflammation, which is often accompanied by complement C3 formation and subsequent cell proliferation and extracellular matrix accumulation in the renal cortex and medulla. In essence, IgAN results in glomerulosclerosis, tubular atrophy, and fibrosis with renal capillary damage, ultimately leading to a complete loss of renal function and the need for hemodialysis.[3,4] However, the complex pathomechanism of IgAN is still not fully understood.[5]

For the diagnosis and monitoring of IgAN, serological and urinary parameters, such as estimated glomerular filtration rate (eGFR), proteinuria, and protein-to-creatinine ratio, are used.[6,7] Unfortunately, these parameters are unspecific for IgAN.[4,8] Histopathological classification based on the demonstration of mesangial immunoglobulin A deposits is considered the criterion standard for the diagnosis of IgAN.[9–11] However, biopsy is limited to sampling error and to its invasive nature, which may entail complications such as postprocedural pain (2%–4%), hematuria (3%–18%), and bleeding (1%–7%).[12–14] Therefore, noninvasive methods are needed to detect structural changes in renal disease and follow-up examinations.

Magnetic resonance elastography (MRE) has gained increasing attention for its noninvasiveness and sensitivity to structural changes in pathologically changed soft tissues[15,16] and has been used for evaluation of healthy native kidneys,[16–18] renal tumors,[19] and renal transplants with chronic insufficiency.[20] Tomoelastography[21] is a recently introduced MRE technique using wave fields at multiple frequencies[17] combined with noise-robust shear wave speed (SWS) recovery based on single-order derivatives and multifrequency SWS compounding.[21–23] As a result, tomoelastography provides highly detailed full-field-of-view SWS maps of renal tissue including anatomical subregions such as cortex and medulla.[17,18]

Besides MRE, there are other promising quantitative magnetic resonance imaging (MRI) techniques that have been used for the detection of renal diseases,[24–26] including diffusion-weighted imaging (DWI) and blood oxygen level–dependent (BOLD) imaging.[27–29] Diffusion-weighted imaging quantifies the diffusivity of water molecules based on the apparent diffusion coefficient (ADC).[30,31] Blood oxygen level–dependent imaging detects changes in inhomogeneous transverse relaxation time T2* due to paramagnetic effects of deoxyhemoglobin, which provide information on the oxygen context of the tissue.[24,25,32]

The aim of this study was to noninvasively examine renal structural and functional changes in patients with IgAN using tomoelastography in combination with DWI and BOLD imaging techniques, which are known to be sensitive to microstructural and oxygenation changes in soft biological tissues, and to assess their diagnostic performance in the detection of IgAN.

MATERIALS AND METHODS

Study Population

Our prospective study was approved by the local ethics committee, and written informed consent was obtained from all subjects. From August 2016 to March 2017, a total of 32 subjects—16 consecutive patients with biopsy-proven IgAN (mean age, 46.1 ± 11.3 years; age range, 24–65 years; 3 females) and 16 age- and sex-matched healthy volunteers (CTR; mean age, 40.5 ± 10.3 years; age range, 28–54 years;

Received for publication February 16, 2019; and accepted for publication, after revision, April 25, 2019.
From the Departments of *Radiology, †Rheumatology, and ‡Nephrology, and §Institute of Medical Informatics, Charité – Universitätsmedizin Berlin, coporate member of Freie Universität Berlin, Humboldt-Universität zu Berlin, and Berlin Institute of Health, Berlin, Germany.
Conflict of interest and sources of funding: This study was supported by the German Federal Ministry of Education and Research (LiSyM 031 L0057 to I.S.) and the German Research Foundation (DFG GU 1726/1-1 to J.G., BIOQIC GRK 2260 to I.S., SFB 1340 to B.H., I.S., J.B., and J.G.).
Correspondence to: Stephan Rodrigo Marticorena Garcia, MD, Department of Radiology, Charité – Universitätsmedizin Berlin, coporate member of Freie Universität Berlin, Humboldt-Universität zu Berlin, and Berlin Institute of Health, Charitéplatz 1, 10117 Berlin, Germany. E-mail: stephan.marticorena-garcia@charite.de.

ISSN: 0020-9996/19/0000–0000
DOI: 10.1097/RLI.0000000000000585

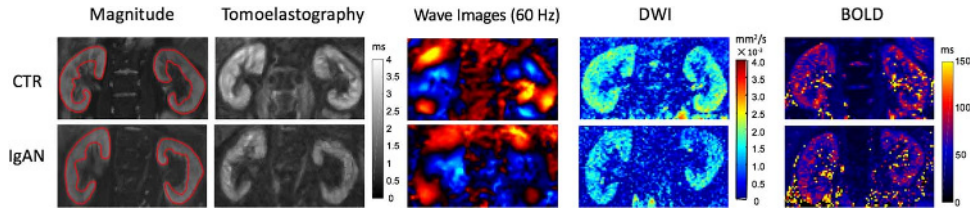

FIGURE 1. Magnitude images of the MRE scan, tomoelastography shear wave speed maps, wave images at 60 Hz, DWI, and BOLD imaging of a healthy control (CTR) and a patient with immunoglobulin A nephropathy (IgAN) and stage 2 chronic kidney disease (eGFR, 89–60 mL/min/1.73 m^2). A marked decrease in SWS and ADC is visible in IgAN, whereas T2* values appear to be only marginally lower in IgAN. Representative regions of interest (ROIs) are demarcated for the entire renal parenchyma comprising cortical and medullar regions (red lines).

5 females)—were examined and enrolled in our study. The inclusion criterion for patients was a history of histopathologically proven IgAN based on renal immunofluorescence analysis without a prior history of urinary disorders, infection, history of malignancy, polycystic kidney disease, hydronephrosis, infarction, and general contraindications to MRI. Inclusion criteria for CTR were no existing history of renal or cardiovascular diseases. All subjects were examined after fasting for 2 hours.

Magnetic Resonance Imaging

Tomoelastography was performed on a 1.5 T MRI scanner (Magnetom Sonata; Siemens) using a 12-channel phased-array surface coil as described in the study of Marticorena Garcia et al.[18] All subjects were examined in supine position using 2 posterior actuators placed underneath each kidney and powered by medical compressed air (0.6 bar). External mechanical vibrations with frequencies of 40, 50, 60, and 70 Hz were used.

The 3-dimensional wave field was acquired using a multislice, single-shot, spin echo planar imaging (EPI) sequence with flow-compensated motion-encoding gradients (MEGs) and fractional encoding optimized according to Dittmann et al.[17] Eight wave phase offsets were recorded for each of the 3 motion directions. The imaging volume consisted of 11 contiguous paracoronal slices through both kidneys with a field of view of 260 × 260 mm^2 (matrix size, 104 × 104) and 2.5 × 2.5 × 2.5 mm^3 voxel size. To increase the signal-to-noise ratio, the signal was averaged over 2 repetitions. Further imaging parameters were as follows: repetition time, 1200 milliseconds; echo time, 55 milliseconds; parallel imaging with a GRAPPA factor of 2; MEG frequency, 48.45 Hz for mechanical frequencies of 40 Hz, 50 Hz, and 60 Hz, and 52.41 Hz for mechanical frequency of 70 Hz; and MEG amplitude of 25 mT/m. The full set of tomoelastography data was acquired within 4 minutes with subjects breathing freely.

For postprocessing, a *k*-MDEV reconstruction method to produce SWS maps (in meter per second) was used, as detailed in Dittmann et al.[17] *k*-MDEV-processing retrieved SWS. Therefore, the complex MRI signal was smoothed by a Gaussian kernel with 2.75 mm of standard deviation before unwrapping. Then a 2-dimensional directional filtering was applied to the unwrapped wave images before inversion. This preprocessing procedure is described in greater detail in Tzschätzsch et al.[21] Furthermore, the loss angle of the complex shear modulus (φ in rad), which is related to solid-fluid soft tissue behavior, was analyzed.[33] φ was obtained from the MDEV processing pipeline. Therefore, a 2-dimensional Butterworth low-pass filter with a threshold of 50 m^{-1} was applied before inversion, as described in the study of Guo et al.[34] The entire postprocessing pipeline is publicly available at www.bioqic-apps.charite.de. The wave speed maps mainly represent tissue stiffness, which in turn is the magnitude of the complex-valued SWS that is related to both elasticity and viscosity. Henceforth, we use "stiffness" to refer to SWS, and the corresponding SWS maps will be denoted as "elastograms," which is the usual term used in the literature.[15]

Diffusion-weighted imaging and BOLD imaging were performed with a spin-EPI sequence and multiple gradient-recalled echo sequence. For DWI, 11 slices with 2.7 × 2.7 × 5 mm^3 resolution were recorded with 2 averages and b-values of 0 and 500 s/mm^2 in 17 seconds. Blood oxygen level–dependent imaging was performed for 3 slices with 2.8 × 2.8 × 5 mm^3 resolution using 8 echo times (2.38–37.72 milliseconds) in 20 seconds.

Regions of interest (ROIs) were manually drawn by 2 observers (observer 1 and 2) for full renal parenchyma, excluding the renal hilus. Regions of interest for tomoelastography, DWI, and BOLD were drawn independently based on paracoronar magnitude images (tomoelastography, combined with corresponding elastograms). Exemplary ROIs are provided in magnitude images in Figure 1.

Clinical Parameters

Renal function was determined as eGFR, which was calculated from blood creatinine levels using the Chronic Kidney Disease Epidemiology Collaboration (CKD-EPI) equation.[35] Urine protein-to-urine creatinine ratio was derived from urine samples as a measure of glomerular damage. All clinical parameters were collected according to standard clinical routine procedures within a maximum interval of 21 days before or after MRI and were analyzed retrospectively.

Statistical Data Analysis

Initially, a 2-sided power analysis was performed to determine the minimum required sample size (alpha value of 0.05, beta value of 0.02, power of 0.8). For each subject, a mean value of the right and left kidney was calculated. Group mean values were reported as means and standard errors of the ROI-averaged values. Intergroup comparison of tomoelastography, DWI, and BOLD results was performed using the

TABLE 1. Characteristics of Controls and Patients

Characteristics	Control n = 16	IgAN n = 16
Sex (female)	5	3
Age, y	41 ± 10	46 ± 11
Body mass index, kg/m^2	22 ± 3	24 ± 4
Heart rate, bpm	67 ± 9	68 ± 12
Systolic blood pressure, mm Hg	126 ± 13	137 ± 13
Diastolic blood pressure, mm Hg	82 ± 6	87 ± 8
eGFR, mL/min/1.73 m^2		39 ± 36
Urine protein to creatinine ratio, mg/g		1179 ± 1104
Time interval: biopsy-tomoelastography, y		10.4 ± 6.2
Patient distribution by CKD stage, %	CKD 1 = 6; CKD 2 = 31; CKD 3 = 13; CKD 4 = 6; CKD 5 = 44.	

IgAN indicates immunoglobulin A nephropathy; eGFR, estimated glomerular filtration rate; CKD, chronic kidney disease.

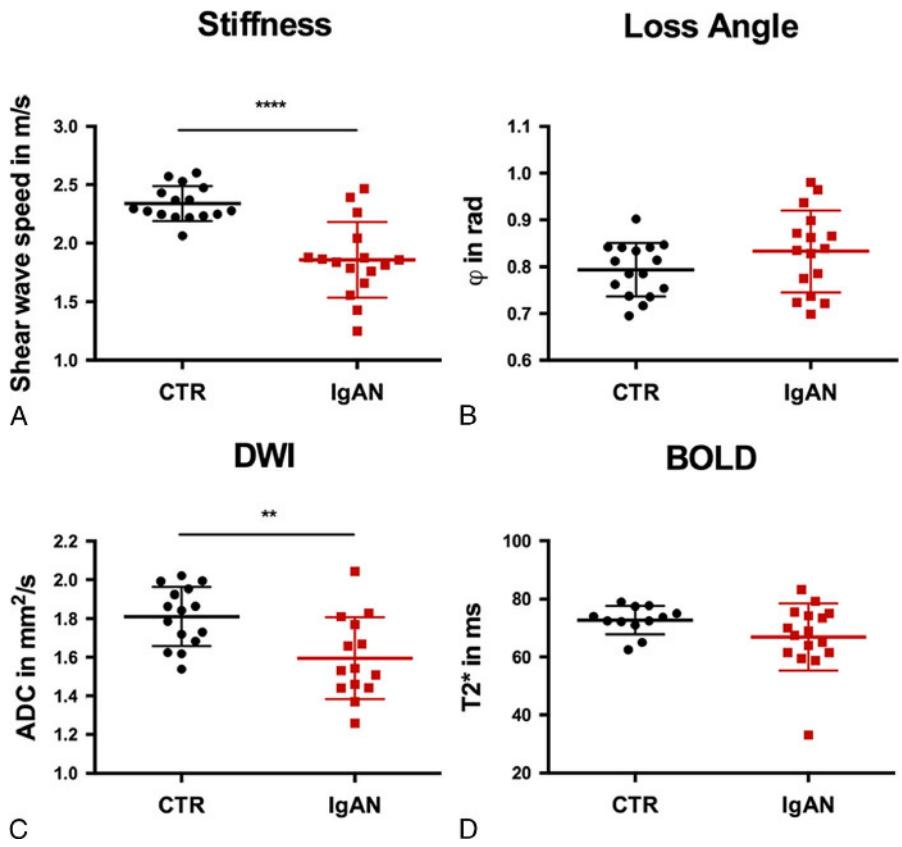

FIGURE 2. Group values of healthy controls (CTR, black dots) and patients with immunoglobulin A nephropathy (IgAN, red squares). Shear wave speed (A) and ADC values (C) are significantly lower in IgAN. No significant differences in φ (B) and T2* values (D).

unpaired Student's *t* test. The diagnostic accuracy of distinguishing IgAN from CTR was assessed using the area under the receiver operating characteristic (AUC) curve analysis. Optimal cutoffs were identified by maximizing the sum of sensitivities and specificities. Interobserver variability was assessed by intraclass correlation coefficient. Correlations between MRI (tomoelastography, DWI, BOLD imaging) and clinical parameters (eGFR, protein-to-creatinine ratio) were analyzed by Pearson's linear correlation coefficient. Statistical analysis was performed using GraphPad Prism v.6 (GraphPad software). *P* values below 0.05 were considered statistically significant.

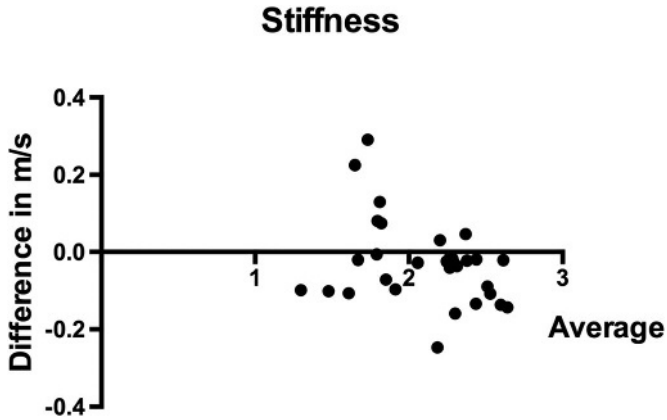

FIGURE 3. Interobserver agreement. Bland-Altman graphs plotting interobserver differences against their average.

RESULTS

Tomoelastography, DWI, and BOLD imaging were performed successfully in both kidneys in 100%, 91%, and 87% of all patients, respectively. Detailed characteristics of healthy controls and patients with IgAN are summarized in Table 1.

Magnetic Resonance Imaging

Representative images of tomoelastography, DWI, and BOLD are shown in Figure 1. Group mean SWS values were significantly lower in IgAN (1.86 ± 0.32 m/s) compared with CTR (2.34 ± 0.15 m/s; $P < 0.0001$), see Figure 2A. Apparent diffusion coefficient values were also lower in IgAN ($1.60 \pm 0.21 \times 10^{-3}$ mm^2/s) compared with CTR ($1.81 \pm 0.15 \times 10^{-3}$ mm^2/s; $P = 0.004$), see Figure 2B. No significant differences were observed between patients with IgAN and CTR for φ (0.79 ± 0.06 rad vs 0.83 ± 0.09 rad; $P = 0.15$) and T2* values (66.91 ± 11.58 milliseconds vs 72.73 ± 4.89 milliseconds; $P = 0.12$),

TABLE 2. Metrics of Magnetic Resonance Imaging

	Control	IgAN	*P*
Shear wave speed, m/s	2.34 ± 0.15	1.86 ± 0.32	<0.0001
Complex shear modulus, φ in rad	0.79 ± 0.06	0.83 ± 0.09	0.15
Apparent diffusion coefficient, $\times 10^{-3}$ mm^2/s	1.81 ± 0.15	1.60 ± 0.21	0.004
T2* relaxation time, ms	72.73 ± 4.89	66.91 ± 11.58	0.12

IgAN indicates immunoglobulin A nephropathy.

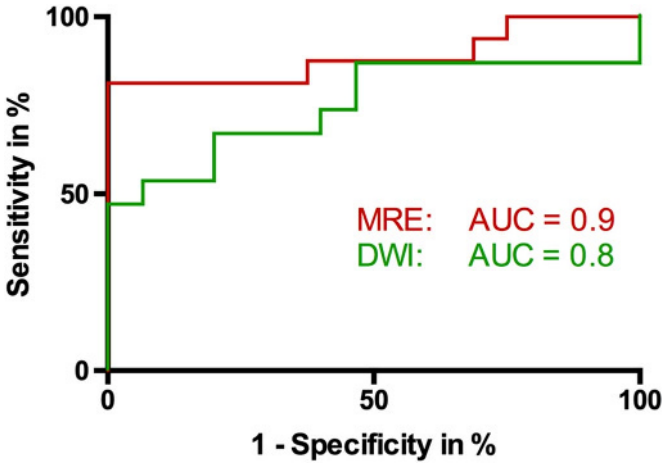

FIGURE 4. MRE (red line) has a higher area under the receiver operating characteristic (AUC) curve than DWI (green line).

see Figure 2, B and C. An excellent intraclass correlation coefficient of 0.95 was observed for SWS (see Fig. 3). Further details are provided in Table 2.

Diagnostic Performance of MRI Modalities and Comparison With Clinical Parameters

The AUC value for distinguishing IgAN from CTR was higher for tomoelastography (0.9) than DWI (0.8), as demonstrated in Figure 4. For tomoelastography, a cutoff of 2.05 m/s was calculated with 81% sensitivity and 100% specificity compared with 1.68 × 10^{-3} mm^2/s for DWI (71%/80%). Further details are given in Table 3. We also analyzed the correlation of all 3 MRI parameters with clinical findings. A significant correlation was only observed between eGFR and SWS ($r = 0.66$, $P = 0.006$), as shown in Figure 5, whereas ADC ($r = 0.26$, $P = 0.36$) and BOLD ($r = 0.40$, $P = 0.12$) did not correlate with eGFR. The protein-to-creatinine ratio did not correlate with any of the MRI parameters ($P \geq 0.42$).

DISCUSSION

Our study demonstrates that tomoelastography allows sensitive, noninvasive detection of changes in renal viscoelastic properties with an excellent interobserver agreement in patients with IgAN.

Immunoglobulin A nephropathy is characterized by restricted water diffusivity (ADC, −12%), which could be related to interstitial fibrosis associated with disease progression in IgAN.[30,36,37] Our results are consistent with the findings of other studies analyzing ADC values in CKD patients of other entities than IgAN.[38–42] In general, tissue stiffness increases with collagen accumulation. However, we observed a marked softening of renal parenchyma due to IgAN with 21% reduction of SWS. This observation is consistent with recent reports of the sensitivity of tissue stiffness and renal SWS to renal perfusion suggesting renal softening when kidney perfusion is decreased.[18,43] As kidneys are

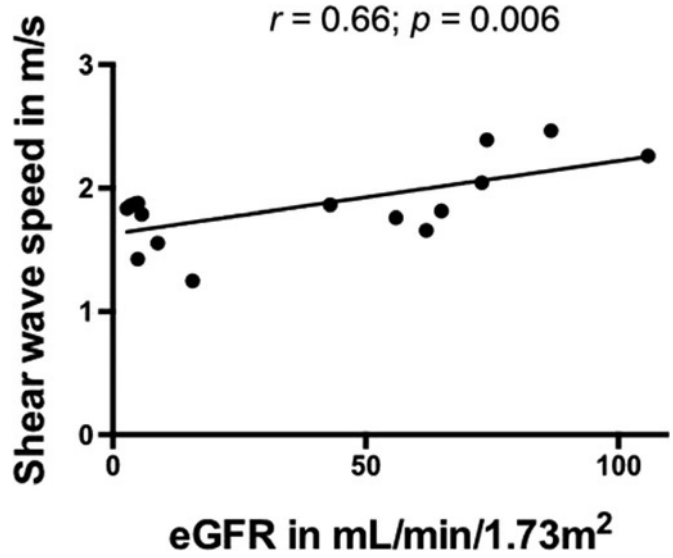

FIGURE 5. Positive correlation of shear wave speed and estimated glomerular filtration rate (eGFR).

highly perfused organs,[44] a possible fibrosis-induced increase in tissue stiffness might be masked by decreased renal perfusion pressure secondary to tubular and glomerular sclerosis and capillary rarefication.[45–48] A positive correlation between eGFR and SWS and a previously reported decrease in renal perfusion in CKD detected by arterial spin labeling MRI[49–52] support our hypothesis. This model of renal softening is sketched in Figure 6, illustrating that dysfunctional kidneys are characterized by decreases in vessel number, diameter, and area[46–48,53] and overall reduced renal perfusion.[49–52] Based on the results of in vivo elastography in different organs at different perfusion states (eg, see Chapter 20 in Sack and Schäffter[58]), we hypothesize that transmural pressure communicates hemodynamic and fluid-mechanical properties such as perfusion pressure[59] into effective-medium stiffness measured by renal tomoelastography. Similar to parameter changes quantified in specimens,[18] an increase of perfusion pressure correlates with an overall stiffening of renal parenchyma presumably due to prestressed microvessels in the kidney. In this model, transmural pressure can be reduced by both a decrease in perfusion and an increase in vessel wall stiffness due to vascular calcification.[54–57] Because of the high vascularization of renal tissue,[44] perfusion pressure has a greater role than fibrosis in determining renal stiffness, leading to an effective drop of stiffness in patients with dysfunctional kidneys. This is confirmed by recent MRI reports of renal softening in native kidneys of patients suffering from lupus nephritis[60] or autosomal dominant polycystic kidney disease[61] and also in chronic kidney graft dysfunction.[20,62] However, to our best knowledge, there are only 3 studies published reporting pathological native kidneys,[19,60,61] one of those[60] with the same tomoelastography setup as presented in this study. Magnetic resonance elastography of native kidney is a relatively new approach;

TABLE 3. Metrics of Diagnostic Performance

	AUC (95% CI)	*P*	Cutoff Value	Sensitivity (95% CI)	Specificity (95% CI)
Shear wave speed, m/s	0.9 (0.8–1.0)	0.0002	2.05	81 (54–96)	100 (79–100)
Complex shear modulus, φ in rad	0.6 (0.4–0.8)	0.2			
Apparent diffusion coefficient, ×10^{-3} mm^2/s	0.8 (0.6–0.1)	0.006	1.68	71 (42–92)	80 (52–96)
T2* relaxation time, ms	0.7	0.14			

AUC indicates area under receiver operating characteristic curve; CI, confidence interval.

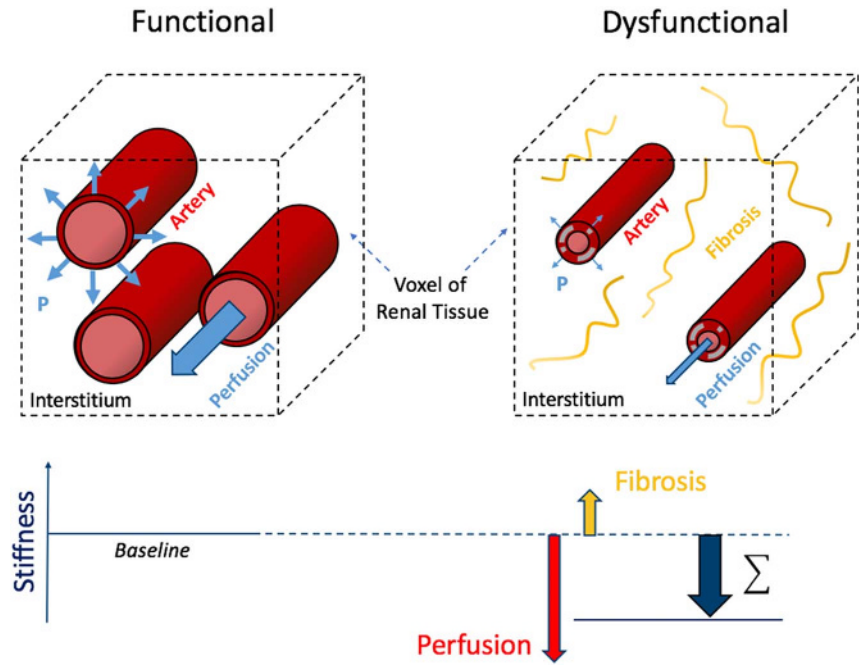

FIGURE 6. Model of renal softening due to reduced perfusion as the predominant factor in dysfunctional kidneys. This model assumes that transmural pressure (P) is reduced by both smaller perfusion[49–52] due to vessel rarefication[46–48,53] and greater stiffness of vessel walls.[54–57] Effective tissue stiffness is sensitive to perfusion pressure.[58] Renal stiffness in dysfunctional kidneys reflects the sum of 2 opposite contributing factors—reduced perfusion pressure (softening, red arrow) and increased interstitial fibrosis (hardening, yellow arrow). Reduced perfusion pressure has a greater effect, resulting in overall renal softening (blue arrow).

therefore the major benefit of this study is to provide quantitative imaging endpoints for further renal examinations.

In our study, BOLD imaging was not sensitive to IgAN, which is possibly attributable to opposed effects in different subregions such as the medulla and cortex[60] consistent to another study analyzing the entire renal parenchyma.[32] To the best of our knowledge, no BOLD analysis has been published in the literature for IgAN detection. Published BOLD studies including patients with chronic kidney disease of different etiologies yield inconsistent data. In agreement with our results, 2 earlier studies did not find a sensitivity of BOLD imaging in chronic kidney disease,[63,64] whereas other authors found significant changes in BOLD imaging in chronic kidney disease.[65–67] This discrepancy could be due to different study protocols, ROI selection, and other factors such as hydration status, pH, and hematocrit, which can also influence magnetic field homogeneity.[68,69]

In our comparison of different MRI modalities, tomoelastography provides a higher diagnostic accuracy than DWI and BOLD in detecting IgAN, suggesting that viscoelastic tissue properties are highly sensitive to chronic kidney disease.

Although promising, our study has limitations. First, the number of patients was small, particularly the subgroup with preserved renal function. Second, subregional analysis was not possible due to the loss of reliable corticomedullary differentiation in atrophic kidneys. Third, renal biopsy data were collected during clinical routine and were analyzed retrospectively. Furthermore, a clinical protocol of DWI was used without utilization of more specific diffusion imaging approaches such as diffusion kurtosis and intravoxel incoherent motion imaging.

In summary, tomoelastography, a multifrequency MRE method, detects renal viscoelastic changes in IgAN with very good diagnostic accuracy. The diagnostic performance of DWI and BOLD imaging, which are known to be sensitive to tissue microstructures and relative hemoglobin oxygenation, is lower. In the future, tomoelastography could be used as a noninvasive and quantitative predictor of structural changes in patients with IgAN. Its noninvasiveness allows implementation in clinical workflow to help clinicians in stratifying patients for renal biopsy and to monitor disease progression.

REFERENCES

1. O'Shaughnessy MM, Hogan SL, Thompson BD, et al. Glomerular disease frequencies by race, sex and region: results from the International Kidney Biopsy Survey. *Nephrol Dial Transplant*. 2018;33:661–669.
2. McGrogan A, Franssen CF, de Vries CS. The incidence of primary glomerulonephritis worldwide: a systematic review of the literature. *Nephrol Dial Transplant*. 2011;26:414–430.
3. Goto M, Wakai K, Kawamura T, et al. A scoring system to predict renal outcome in IgA nephropathy: a nationwide 10-year prospective cohort study. *Nephrol Dial Transplant*. 2009;24:3068–3074.
4. D'Amico G. Natural history of idiopathic IgA nephropathy: role of clinical and histological prognostic factors. *Am J Kidney Dis*. 2000;36:227–237.
5. Knoppova B, Reily C, Maillard N, et al. The origin and activities of IgA1-containing immune complexes in IgA nephropathy. *Front Immunol*. 2016;7:117.
6. Floege J. Primary glomerulonephritis: A review of important recent discoveries. *Kidney Res Clin Pract*. 2013;32:103–110.
7. Rostoker G, Andrivet P, Pham I, et al. Accuracy and limitations of equations for predicting the glomerular filtration rate during follow-up of patients with non-diabetic nephropathies. *BMC Nephrol*. 2009;10:16.
8. Wyatt RJ, Julian BA. IgA nephropathy. *N Engl J Med*. 2013;368:2402–2414.
9. Magistroni R, D'Agati VD, Appel GB, et al. New developments in the genetics, pathogenesis, and therapy of IgA nephropathy. *Kidney Int*. 2015;88:974–989.
10. Working Group of the International IgA Nephropathy Network and the Renal Pathology SocietyCattran DC, Coppo R, et al. The Oxford classification of IgA nephropathy: rationale, clinicopathological correlations, and classification. *Kidney Int*. 2009;76:534–545.
11. Trimarchi H, Barratt J, Cattran DC, et al. Oxford Classification of IgA nephropathy 2016: an update from the IgA Nephropathy Classification Working Group. *Kidney Int*. 2017;91:1014–1021.
12. Roccatello D, Sciascia S, Rossi D, et al. Outpatient percutaneous native renal biopsy: safety profile in a large monocentric cohort. *BMJ Open*. 2017;7:e015243.
13. Lees JS, McQuarrie EP, Mordi N, et al. Risk factors for bleeding complications after nephrologist-performed native renal biopsy. *Clin Kidney J*. 2017;10:573–577.

14. Whittier WL. Complications of the percutaneous kidney biopsy. *Adv Chronic Kidney Dis*. 2012;19:179–187.
15. Hirsch S, Braun J, Sack I. *Magnetic Resonance Elastography: Physical Background and Medical Applications*. Weinheim, Germany: Wiley-VCH; 2017.
16. Venkatesh SK, Ehman RL. Magnetic resonance elastography of abdomen. *Abdom Imaging*. 2015;40:745–759.
17. Dittmann F, Tzschatzsch H, Hirsch S, et al. Tomoelastography of the abdomen: tissue mechanical properties of the liver, spleen, kidney, and pancreas from single MR elastography scans at different hydration states. *Magn Reson Med*. 2017;78: 976–983.
18. Marticorena Garcia SR, Grossmann M, Lang ST, et al. Tomoelastography of the native kidney: regional variation and physiological effects on in vivo renal stiffness. *Magn Reson Med*. 2018;79:2126–2134.
19. Prezzi D, Neji R, Kelly-Morland C, et al. Characterization of small renal tumors with magnetic resonance elastography: a feasibility study. *Invest Radiol*. 2018; 53:344–351.
20. Marticorena Garcia SR, Fischer T, Durr M, et al. Multifrequency magnetic resonance elastography for the assessment of renal allograft function. *Invest Radiol*. 2016;51:591–595.
21. Tzschätzsch H, Guo J, Dittmann F, et al. Tomoelastography by multifrequency wave number recovery from time-harmonic propagating shear waves. *Med Image Anal*. 2016;30:1–10.
22. Manduca A, Lake DS, Kruse SA, et al. Spatio-temporal directional filtering for improved inversion of MR elastography images. *Med Image Anal*. 2003;7:465–473.
23. Manduca A, Oliphant TE, Dresner MA, et al. Magnetic resonance elastography: non-invasive mapping of tissue elasticity. *Med Image Anal*. 2001;5:237–254.
24. Ebrahimi B, Textor SC, Lerman LO. Renal relevant radiology: renal functional magnetic resonance imaging. *Clin J Am Soc Nephrol*. 2014;9:395–405.
25. Zhang JL, Morrell G, Rusinek H, et al. New magnetic resonance imaging methods in nephrology. *Kidney Int*. 2014;85:768–778.
26. Attenberger UI, Morelli J, Budjan J, et al. Fifty years of technological innovation: potential and limitations of current technologies in abdominal magnetic resonance imaging and computed tomography. *Invest Radiol*. 2015;50:584–593.
27. Li X, Xu X, Zhang Q, et al. Diffusion-weighted imaging and blood oxygen level–dependent MR imaging of kidneys in patients with lupus nephritis. *J Transl Med*. 2014;12:295.
28. Rapacchi S, Smith RX, Wang Y, et al. Towards the identification of multi-parametric quantitative MRI biomarkers in lupus nephritis. *Magn Reson Imaging*. 2015;33:1066–1074.
29. Shi H, Yan T, Li D, et al. Detection of renal hypoxia in lupus nephritis using blood oxygen level–dependent MR imaging: a multiple correspondence analysis. *Kidney Blood Press Res*. 2017;42:123–135.
30. Thoeny HC, De Keyzer F, Oyen RH, et al. Diffusion-weighted MR imaging of kidneys in healthy volunteers and patients with parenchymal diseases: initial experience. *Radiology*. 2005;235:911–917.
31. Schmidt H, Gatidis S, Schwenzer NF, et al. Impact of measurement parameters on apparent diffusion coefficient quantification in diffusion-weighted-magnetic resonance imaging. *Invest Radiol*. 2015;50:46–56.
32. Thacker JM, Li LP, Li W, et al. Renal blood oxygenation level-dependent magnetic resonance imaging: a sensitive and objective analysis. *Invest Radiol*. 2015; 50:821–827.
33. Hirsch S, Guo J, Reiter R, et al. MR elastography of the liver and the spleen using a piezoelectric driver, single-shot wave-field acquisition, and multifrequency dual parameter reconstruction. *Magn Reson Med*. 2014;71:267–277.
34. Guo J, Buning C, Schott E, et al. In vivo abdominal magnetic resonance elastography for the assessment of portal hypertension before and after transjugular intrahepatic portosystemic shunt implantation. *Invest Radiol*. 2015;50:347–351.
35. Levey AS, Stevens LA, Schmid CH, et al. A new equation to estimate glomerular filtration rate. *Ann Intern Med*. 2009;150:604–612.
36. Friedli I, Crowe LA, Berchtold L, et al. New magnetic resonance imaging index for renal fibrosis assessment: a comparison between diffusion-weighted imaging and T1 mapping with histological validation. *Sci Rep*. 2016;6:30088.
37. Roberts IS. Pathology of IgA nephropathy. *Nat Rev Nephrol*. 2014;10:445–454.
38. Zhao J, Wang ZJ, Liu M, et al. Assessment of renal fibrosis in chronic kidney disease using diffusion-weighted MRI. *Clin Radiol*. 2014;69:1117–1122.
39. Mao W, Zhou J, Zeng M, et al. Intravoxel incoherent motion diffusion-weighted imaging for the assessment of renal fibrosis of chronic kidney disease: a preliminary study. *Magn Reson Imaging*. 2018;47:118–124.
40. Li Q, Li J, Zhang L, et al. Diffusion-weighted imaging in assessing renal pathology of chronic kidney disease: a preliminary clinical study. *Eur J Radiol*. 2014;83:756–762.
41. Xu X, Palmer SL, Lin X, et al. Diffusion-weighted imaging and pathology of chronic kidney disease: initial study. *Abdom Radiol (NY)*. 2018;43:1749–1755.
42. Toya R, Naganawa S, Kawai H, et al. Correlation between estimated glomerular filtration rate (eGFR) and apparent diffusion coefficient (ADC) values of the kidneys. *Magn Reson Med Sci*. 2010;9:59–64.
43. Warner L, Yin M, Glaser KJ, et al. Noninvasive in vivo assessment of renal tissue elasticity during graded renal ischemia using MR elastography. *Invest Radiol*. 2011;46:509–514.
44. Carlstrom M, Wilcox CS, Arendshorst WJ. Renal autoregulation in health and disease. *Physiol Rev*. 2015;95:405–511.
45. Nangaku M. Mechanisms of tubulointerstitial injury in the kidney: final common pathways to end-stage renal failure. *Intern Med*. 2004;43:9–17.
46. Kramann R, Tanaka M, Humphreys BD. Fluorescence microangiography for quantitative assessment of peritubular capillary changes after AKI in mice. *J Am Soc Nephrol*. 2014;25:1924–1931.
47. Choi YJ, Chakraborty S, Nguyen V, et al. Peritubular capillary loss is associated with chronic tubulointerstitial injury in human kidney: altered expression of vascular endothelial growth factor. *Hum Pathol*. 2000;31:1491–1497.
48. Bohle A, Mackensen-Haen S, Wehrmann M. Significance of postglomerular capillaries in the pathogenesis of chronic renal failure. *Kidney Blood Press Res*. 1996; 19:191–195.
49. Li LP, Tan H, Thacker JM, et al. Evaluation of renal blood flow in chronic kidney disease using arterial spin labeling perfusion magnetic resonance imaging. *Kidney Int Rep*. 2017;2:36–43.
50. Cai YZ, Li ZC, Zuo PL, et al. Diagnostic value of renal perfusion in patients with chronic kidney disease using 3D arterial spin labeling. *J Magn Reson Imaging*. 2017;46:589–594.
51. Lanzman RS, Wittsack HJ, Martirosian P, et al. Quantification of renal allograft perfusion using arterial spin labeling MRI: initial results. *Eur Radiol*. 2010;20:1485–1491.
52. Rossi C, Artunc F, Martirosian P, et al. Histogram analysis of renal arterial spin labeling perfusion data reveals differences between volunteers and patients with mild chronic kidney disease. *Invest Radiol*. 2012;47:490–496.
53. Seron D, Alexopoulos E, Raftery MJ, et al. Number of interstitial capillary cross-sections assessed by monoclonal antibodies: relation to interstitial damage. *Nephrol Dial Transplant*. 1990;5:889–893.
54. Covic A, Kanbay M, Voroneanu L, et al. Vascular calcification in chronic kidney disease. *Clin Sci (Lond)*. 2010;119:111–121.
55. Manzoor S, Ahmed S, Ali A, et al. Progression of medial arterial calcification in CKD. *Kidney Int Rep*. 2018;3:1328–1335.
56. Ogawa T, Nitta K. Pathogenesis and management of vascular calcification in patients with end-stage renal disease. *Contrib Nephrol*. 2018;196:71–77.
57. Reiss AB, Miyawaki N, Moon J, et al. CKD, arterial calcification, atherosclerosis and bone health: inter-relationships and controversies. *Atherosclerosis*. 2018;278:49–59.
58. Sack I, Schäffter T. *Quantification of Biophysical Parameters in Medical Imaging*. Heidelberg, Germany: Springer International Publishing; 2018.
59. Hetzer S, Birr P, Fehlner A, et al. Perfusion alters stiffness of deep gray matter. *J Cereb Blood Flow Metab*. 2018;38:116–125.
60. Marticorena Garcia SR, Grossmann M, Bruns A, et al. Tomoelastography paired with T2* magnetic resonance imaging detects lupus nephritis with normal renal function. *Invest Radiol*. 2019;54:89–97.
61. Kline TL, Edwards ME, Garg I, et al. Quantitative MRI of kidneys in renal disease. *Abdom Radiol (NY)*. 2018;43:629–638.
62. Lee CU, Glockner JF, Glaser KJ, et al. MR elastography in renal transplant patients and correlation with renal allograft biopsy: a feasibility study. *Acad Radiol*. 2012; 19:834–841.
63. Pruijm M, Hofmann L, Piskunowicz M, et al. Determinants of renal tissue oxygenation as measured with BOLD-MRI in chronic kidney disease and hypertension in humans. *PloS One*. 2014;9:e95895.
64. Khatir DS, Pedersen M, Jespersen B, et al. Evaluation of renal blood flow and oxygenation in CKD using magnetic resonance imaging. *Am J Kidney Dis*. 2015;66:402–411.
65. Prasad PV, Thacker J, Li LP, et al. Multi-parametric evaluation of chronic kidney disease by MRI: a preliminary cross-sectional study. *PloS One*. 2015; 10:e0139661.
66. Milani B, Ansaloni A, Sousa-Guimaraes S, et al. Reduction of cortical oxygenation in chronic kidney disease: evidence obtained with a new analysis method of blood oxygenation level-dependent magnetic resonance imaging. *Nephrol Dial Transplant*. 2017;32:2097–2105.
67. Xin-Long P, Jing-Xia X, Jian-Yu L, et al. A preliminary study of blood-oxygen-level-dependent MRI in patients with chronic kidney disease. *Magn Reson Imaging*. 2012;30:330–335.
68. Pruijm M, Milani B, Burnier M. Blood oxygenation level-dependent MRI to assess renal oxygenation in renal diseases: progresses and challenges. *Front Physiol*. 2016;7:667.
69. Neugarten J. Renal BOLD-MRI and assessment for renal hypoxia. *Kidney Int*. 2012;81:613–614.